Predominance of transfer in triggering breakup in sub-barrier reactions of ^{6,7}Li with ^{144}Sm, ^{207,208}Pb, and ^{209}Bi

D. H. Luong,[1] M. Dasgupta,[1] D. J. Hinde,[1] R. du Rietz,[1,*] R. Rafiei,[1,†] C. J. Lin,[1,‡] M. Evers,[1] and A. Diaz-Torres[2]
[1]*Department of Nuclear Physics, Research School of Physics and Engineering, Australian National University, Canberra, ACT 0200, Australia*
[2]*ECT**, *Villa Tambosi, I-38123 Villazzano, Trento, Italy*

(Received 25 June 2013; revised manuscript received 15 August 2013; published 24 September 2013)

Coincidence measurements of breakup fragments were carried out for the ^{7}Li + ^{144}Sm and ^{6,7}Li + ^{207,208}Pb,^{209}Bi reactions at sub-barrier energies. Breakup modes in reactions of ^{6,7}Li were identified through the reaction Q values, and the time-scales of each process inferred through the relative energy of the breakup fragments. Breakup was found to be predominantly triggered by nucleon transfer, with p pickup leading to $\alpha + \alpha$ coincidences being the preferred breakup mode for ^{7}Li, and n stripping leading to $\alpha + p$ for ^{6}Li. Breakup triggered by $2n$ stripping was also found to be prominent in the ^{7}Li + ^{144}Sm reaction. The breakup yields were separated into prompt and delayed components based on the relative energies of the breakup fragments. This enables the identification of breakup process important in the suppression of complete fusion of ^{6,7}Li at above-barrier energies.

DOI: 10.1103/PhysRevC.88.034609 PACS number(s): 25.70.Hi, 25.70.Mn, 21.60.Gx

I. INTRODUCTION

With the discovery of halo nuclei [1,2] and the recent advent around the world of pure beams of radioactive ions, there is a global push to resolve the cognate challenge of understanding interactions of their weakly bound stable cousins. Exploiting the experimental barrier distribution [3,4], it was clearly demonstrated that complete fusion (CF) of the weakly bound nuclei ^{6,7}Li and ^{9}Be with heavy target nuclei is suppressed by $\sim$30% [5–7] at above-barrier energies. This observed suppression of CF has been widely associated [5–15] with the breakup of ^{6,7}Li and ^{9}Be, due to their low threshold energies for breakup, resulting in the loss of flux of intact nuclei at the fusion barrier. The mechanism for breakup of weakly bound nuclei was commonly expected [16–19] to be through cluster decay from unbound states of the projectile. Qualitatively, coupling to channels leading to breakup was shown [20] to suppress CF at above-barrier energies. More realistic modeling of the interplay between breakup and CF requires the incorporation of the mechanisms triggering breakup, and post-breakup trajectories of the fragments [21]. To simplify the determination of the breakup mechanism experimentally, coincidence measurements of breakup fragments of ^{6,7}Li and ^{9}Be were performed at sub-barrier energies [22–27] (choosing sub-barrier energies minimise the probability of fragment capture, thus maximise the probability of detecting all breakup fragments). These studies revealed the presence of competing reaction channels such as nucleon-transfer leading to breakup of the projectile-like nuclei. For ^{9}Be, neutron-stripping is the dominant trigger for breakup [26,28]. The sub-barrier breakup probability was observed to depend exponentially on the projectile-target separation, allowing extrapolation to the smaller separation distances at above-barrier energies [23,26,28]. This allowed increasingly quantitative relationships to be established between sub-barrier breakup probabilities and above-barrier suppression of CF through calculation of CF and incomplete fusion (ICF) yields using PLATYPUS [29–31], a three-dimensional classical trajectory model. Knowledge of the reaction processes leading to breakup at sub-barrier energies is not sufficient to relate it to above-barrier suppression of CF. These works [23,26,27,32] have pointed out that it is critical to also know the time-scale of each of these breakup mechanisms in relation to the fusion time-scale. If the projectile, or projectile-like nucleus, is excited to a state with a lifetime longer than the fusion time-scale, in collisions at above-barrier energies, these nuclei can arrive at the barrier radius intact and undergo fusion. It is only the *prompt* [23,26] breakup components, i.e., breakup of the projectile before reaching the barrier radius, that can compete with and suppress CF.

To extend the investigation of the mechanisms of sub-barrier breakup in reactions of ^{6,7}Li and identify the prompt breakup components, this paper describes sub-barrier coincidence measurements of breakup fragments in the reactions of ^{7}Li with ^{144}Sm, and ^{6,7}Li with ^{207,208}Pb and ^{209}Bi. The mechanisms for breakup, and their time-scales, were identified through the reaction Q values and the relative energy of the surviving or noncaptured breakup fragments. Relative probabilities for sub-barrier prompt breakup processes fast enough ($\sim 10^{-22}$ s) to affect fusion are presented.

II. EXPERIMENTAL SETUP AND ANALYSIS PROCEDURE

Beams of ^{6,7}Li were provided by the 14UD electrostatic accelerator at the Australian National University. They were

---

*Current address: Malmö University, Faculty of Technology and Society, 205 06 Malmö, Sweden.

†Current address: School of Electrical, Electronic and Computer Engineering, The University of Western Australia, Perth, WA 6009, Australia.

‡Current address: China Institute of Atomic Energy, Beijing 102413, China.

TABLE I. Beam energies at which measurements were made for the reactions of ^{6}Li with indicated targets. $E_{c.m.}$ is the center-of-mass energy of the system, and includes energy loss in the target.

Target	V_b (MeV)	E_{beam} (MeV)	$E_{c.m.}$ (MeV)	$E_{c.m.}/V_b$
^{207}Pb	29.80[a]	26.5	25.74	0.86
		29.0	28.17	0.94
^{208}Pb	29.76[a]	26.5	25.73	0.86
		29.0	28.16	0.95
^{209}Bi	30.10[b]	26.5	25.74	0.85
		29.0	28.17	0.93

[a]Scaled barrier as described in Ref. [33].
[b]Measured barrier from Ref. [6].

incident on a 99.0% enriched ^{207}PbS target, 70 μg cm^{-2} in thickness, a 98.7% enriched ^{208}PbS target, 170 μg cm^{-2} in thickness, a 130 μg cm^{-2} thick ^{209}Bi target, and a 100 μg cm^{-2} thick ^{144}Sm target. All targets had a carbon backing, $\sim$15 μg cm^{-2} thick, facing downstream of the incident beam. The beam energies and target combination are listed in Tables I and II, along with the center-of-mass barrier energy V_b for each reaction.

Charged breakup fragments from the reaction were captured in coincidence using BALIN [35], a detector array consisting of four large area double-sided silicon strip detectors (DSSDs) from Micron Semiconductor Ltd. Each was 400 μm in thickness, with 16 arcs and eight sectors, giving 128 position pixels. The silicon dead layers of each DSSD were measured to be $\sim$2 μm, with an additional 0.2 μm of aluminium coating. Three DSSDs were arranged in a lamp-shade configuration with apex angle 45° as illustrated in Fig. 1(a). The central DSSD, labeled ΔE-E, had an identical DSSD placed 5mm behind it to create a detector telescope. This allowed the identification of isotopes of hydrogen, as shown in Fig. 1(b), as well as the determination of the energy of the longest range protons, which extended up to 20 MeV. For the given detector thickness, energy loss calculations performed using SRIM [36] predicted that high-Z particles, α particles, and low energy protons (<7.0 MeV), deuterons (<9.0 MeV), and

TABLE II. Beam energies at which measurements were made for the reactions of ^{7}Li with indicated targets. $E_{c.m.}$ is the center-of-mass energy of the system, and includes energy loss in the target.

Target	V_b (MeV)	E_{beam} (MeV)	$E_{c.m.}$ (MeV)	$E_{c.m.}/V_b$
^{144}Sm	23.63[a]	21.5	20.47	0.87
		24.0	22.87	0.97
^{207}Pb	29.43[b]	24.0	23.20	0.79
		26.5	25.62	0.87
		29.0	28.04	0.95
^{208}Pb	29.40[b]	24.0	23.21	0.80
		29.0	28.03	0.95
^{209}Bi	29.70[c]	24.0	23.20	0.78
		29.0	28.04	0.94

[a]São Paulo potential [34].
[b]Scaled barrier as described in Ref. [33].
[c]Measured barrier from Ref. [6].

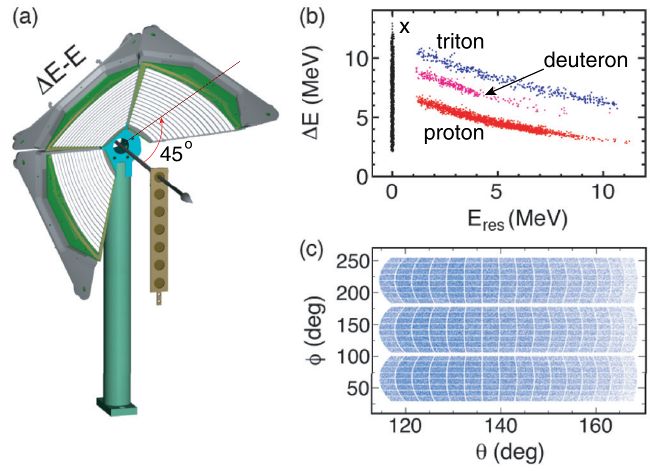

FIG. 1. (Color online) (a) Arrangement of the detector array of four DSSDs, with the beam (arrow) and target ladder. The central detector element, labeled ΔE-E, contains two DSSDs back to back. (b) Typical energy loss ΔE vs. residual energy E_{res} recorded by the back element of the detector telescope, for protons, deuterons, and tritons. Particles (x) that deposit all their energy in the first (ΔE) detector cannot be identified individually, but are identified through the kinematic reconstruction of the breakup event. (c) The array covers 50° in scattering angle θ and 210° in azimuthal angle ϕ. Pixel separation in each detector is exaggerated for clarity.

tritons (<11.0 MeV) would stop completely inside the front element of the telescope and thus would not be individually identified. They can however be identified through kinematic reconstruction of the breakup event, as will be demonstrated in Sec. III.

The position identification characteristics of the DSSDs does not allow position location within the pixel. However, to simplify subsequent event reconstruction a position was assumed by randomisation, taking a uniform distribution of the position within the physical boundaries of the pixel. A mylar foil of 0.7 μm thickness was placed in front of the DSSDs to stop low energy electrons. The array was also shielded by an aluminium sheet from seeing scattered beam particles interacting downstream of the target. Individual energy calibration of each of the 64 arcs and 32 sectors of the DSSDs was made utilising scattered Li and proton beams, and decay α particles. The kinetic energy E_i of the particles was taken from the energy signal from the arcs, whose resolution of $\lesssim$0.1 MeV FWHM was better than the sectors. Energy loss of a particle traversing the aforementioned detector dead layer, aluminium coating and mylar foil was accounted for event-by-event, both in the energy calibrations, and in the breakup measurements.

The detector array was placed at backward angles, covering scattering angles from 117° to 167°, and spanning 210° in azimuthal angle as shown in Fig. 1(c). This gave three experimental advantages. (i) The backward angle placement minimised the rate of elastically scattered beam particles. (ii) Contributions to the singles rate from reactions with low-Z impurities in the target such as carbon, oxygen, and sulfur were minimized. A measurement with a carbon target showed that the kinematical reconstruction method completely eliminates interference from such reactions. (iii) It was shown experimentally [17,37–39] that at sub-barrier energies, reaction products associated with breakup and/or transfer, such as α particles, show peak yields of $d\sigma/d\Omega$ at backward angles. The Coulomb deflection function shows that the trajectories with the smallest impact parameters and internuclear separations are found around 180°. The probabilities of breakup through all mechanism have been shown to depend exponentially on the proximity of the nuclear surfaces [23,26]. Thus the highest breakup probabilities are associated with low impact parameter collisions. The associated breakup fragments will be at backward angles, as long as they are not absorbed. This will be the case at below-barrier energies. The large angular coverage, in both scattering and azimuthal angles, means that we are sensitive to all breakup modes.

For breakup of ^{6}Li and ^{7}Li, the most energetically favored breakup modes involve the production of two charged fragments, $\alpha + d$ and $\alpha + t$, respectively [40]. Hence, to minimize the data collection rate during breakup measurements, data were recorded only when any two arcs from the whole detector array fired. The count rates were generally kept at $\lesssim$500 counts/s, corresponding to a deadtime of $\sim$6%.

A. Extraction of breakup events

The energies E_i recorded for binary coincidence particles i from the reaction of ^{7}Li with ^{207}Pb at $E_{\text{beam}} = 29.0$ MeV are presented as two-dimensional E_1 vs. E_2 spectra in Fig. 2. Events that do not include information from the back element of the detector telescope, and thus both coincidence particles are mass-unidentified, are shown in Fig. 2(a). Coincidences where one of the complementary particles is identified as a hydrogen isotope by the detector telescope are shown in Fig. 2(b). Figure 2(c) combines data from both Fig. 2(a) and Fig. 2(b), showing the common features in mass-unidentified and identified events. The ordering between the two particles (E_1 or E_2) was randomised at this stage, resulting in a symmetric distribution about 45°, but not mirror-symmetric, as each binary event is only plotted once. The structures that emerge from these spectra include groups of events forming distinct diagonal bands showing particle pairs with a common origin and correlated energies, e.g., binary breakup pairs (labeled A to D), and horizontal and vertical bands labeled E.

In Fig. 2(a), events in band E are random coincidences with elastically scattered beam particles. Band A comprises events where the sum energy ($E_1 + E_2$) of the coincident particles is equal to that of elastically scattered ^{7}Li. These events are false coincidences arising due to *elastic cross-talk* where ^{7}Li was incident on an arc boundary, causing charge to be collected on two adjacent arcs resulting in this band. However, when events involving coincidences of adjacent pixels, whose sum energy approximately equals that of elastically scattered Li, are gated out then band A is completely removed as can be seen in Fig. 2(c). This process is applied to all data presented in this paper.

Events forming the diagonal bands B are $\alpha + d$ coincidences. Events with complete energy deposition of the high energy deuteron in the ΔE-E telescope are shown in Fig. 2(b). Figure 2(a) includes events with low energy deuterons, and events with incomplete energy deposition of high energy deuterons. If these long-range deuterons are incident on a non-telescope detector, only their energy loss is recorded, which is a maximum of 10 MeV. This results in a discontinuity between $10 < E_{1,2} < 12.5$ MeV at which the straight line of bands B is replaced by two arcs. The alignment of the bands B in Fig. 2(c) confirms that these are $\alpha + d$ coincidences.

In Fig. 2(a), events in band C have reduced intensity at $E_{1,2} > 11.5$ MeV, the maximum energy a *triton* can deposit in the DSSD. By overlaying this band with coincidences with an identified triton, the black band in Fig. 2(b), the alignment of the two bands can be seen in Fig. 2(c). This indicates that events in band C are $\alpha + t$ coincidences. The diagonal band

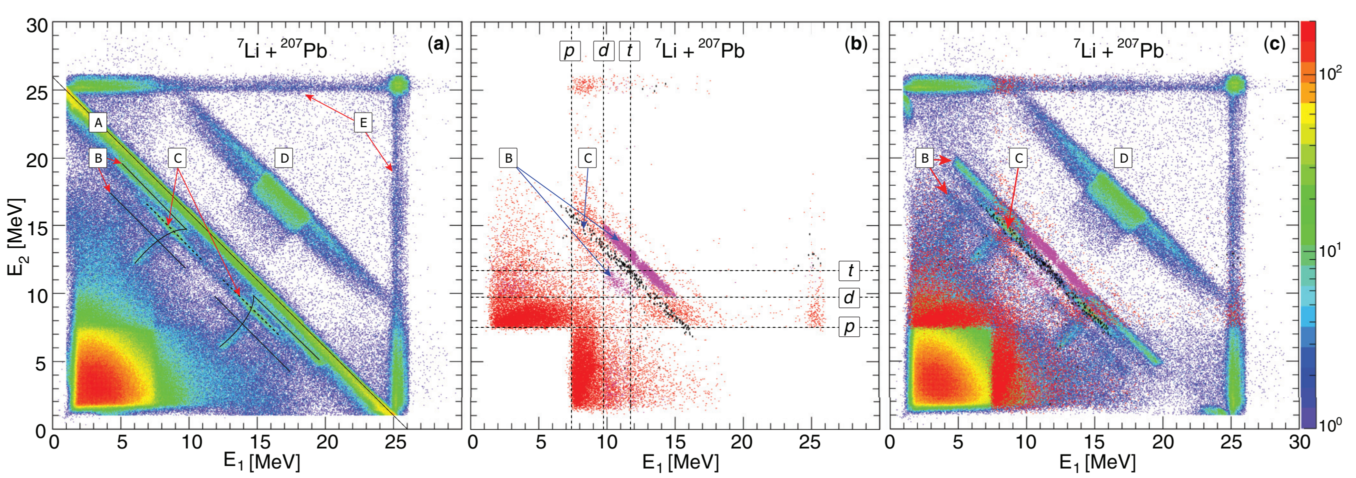

FIG. 2. (Color online) Two-dimensional E_1 vs. E_2 spectra for binary coincidence events from the reaction of ^{7}Li with ^{207}Pb at $E_{\text{beam}} = 29.0$ MeV. Symmetry about 45° is a result of random ordering of the coincident particles. (a) Spectrum where both coincidence particles are unidentified. Events from elastic cross-talk are labeled A. (b) Spectrum where one of the coincidence particles has been identified as either a proton (red), deuteron (magenta), or triton (black). Dashed lines indicate the lower energy limit needed to identify the three hydrogen isotopes. (c) Mass-unidentified events from (b) have been overlaid on top of mass-identified events from (a). Elastic cross-talk events have also been eliminated (see text).

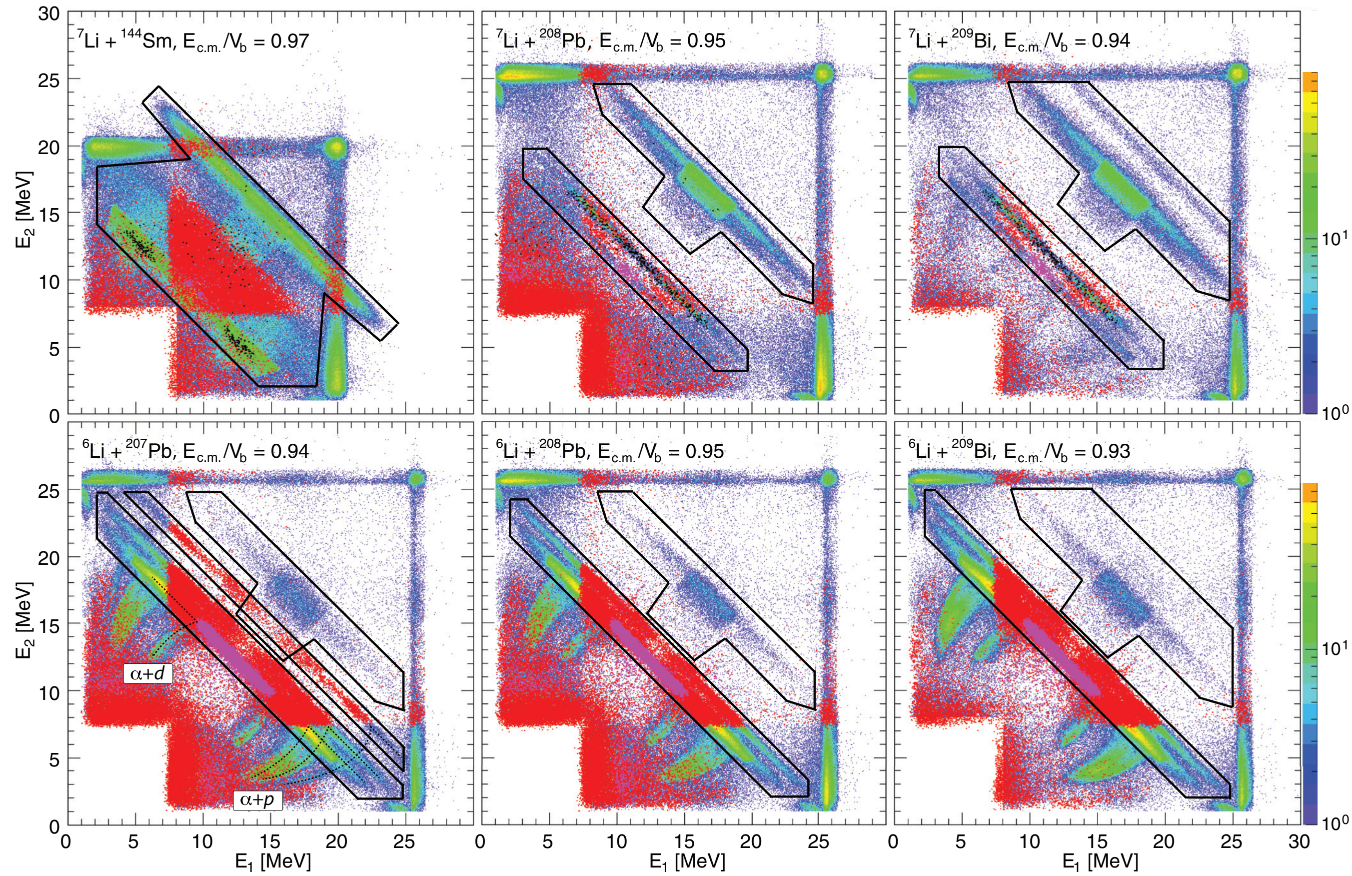

FIG. 3. (Color online) Two-dimensional E_1 vs. E_2 spectra for binary coincidence events from the reaction of ^{7}Li with ^{144}Sm at $E_{\rm beam} =$ 24.0 MeV, and ^{6,7}Li with ^{207,208}Pb and ^{209}Bi at $E_{\rm beam} = 29.0$ MeV. Mass-unidentified events (intensity scale at the right) where both coincidence particles have energy lower than 8 MeV have been removed, together with elastic cross-talk. Overlaid on the mass-unidentified events are events where one of the coincident particles has been identified as a proton (red), deuteron (magenta), and triton (black). This color scheme is independent of the intensity scale for the mass-unidentified events. Symmetry about 45° is a result of random ordering of the coincident particles. Events forming arcs, as indicated by broken lines labeled $\alpha + d$ and $\alpha + p$ in the bottom left figure, are $\alpha + d$ and $\alpha + p$ coincidences where the deuteron or proton was incident on the nontelescopic section of the detector array, resulting in incomplete energy deposition. This feature is common to all reactions with the ^{6}Li projectile. The black polygons are gates for correlated events with full energy deposition, and define the lower cutoff in Q value for Fig. 4. The authors are aware that these gates are not perfect, as they cannot eliminate all possible backgrounds—as in the case for ^{7}Li + ^{144}Sm—or include all genuine $\alpha + \alpha$ coincidences as for the reaction ^{7}Li + ^{209}Bi.

D is continuous throughout, indicating that events in this band correspond to both coincident particles always being stopped in the 400 μm DSSDs. This must correspond to both particles having mass larger than that of a triton. The most likely origin is $\alpha + \alpha$ coincidences from a ^{8}Be parent-nucleus. Such a reaction would involve p pickup by ^{7}Li to produce ^{8}Be, which has a large positive Q value (+9.86 MeV), consistent with the sum energies $E_1 + E_2 \gg E_{\rm beam}$.

Shown in Fig. 3 are two-dimensional E_1 vs. E_2 spectra for binary coincidences, of mass-unidentified events overlaid with mass-identified events, from the reactions of ^{7}Li with ^{144}Sm at $E_{\rm beam} = 24.0$ MeV and ^{6,7}Li with ^{207,208}Pb and ^{209}Bi at $E_{\rm beam} = 29.0$ MeV. The spectra recorded at other (lower) beam energies show similar features, but with reduced yields (see for example the reaction of ^{7}Li with ^{207}Pb in Fig. 6). All the structures that appear are similar to those seen and discussed in Fig. 2, namely diagonal bands consisting of events with correlated energies, and arcs arising from incomplete energy deposition of high energy hydrogen isotopes. The arcs starting at 7.5 MeV (*proton*) and 10 MeV (*deuteron*), most prominent in reactions with ^{6}Li, are formed from incomplete energy deposition in coincidences with high energy protons or deuterons incident on the nontelescope element part of the detector array. Coincidences identified by the ΔE-E telescope as $\alpha + p$ are overlaid in red, $\alpha + d$ in magenta and $\alpha + t$ in black, allowing the confirmation of $\alpha + p$ and $\alpha + d$ coincidences for ^{6}Li-induced reactions and $\alpha + p$, $\alpha + d$ and $\alpha + t$ coincidences for reactions with ^{7}Li. Events indicative of $\alpha + \alpha$ coincidences are seen in both ^{6}Li- and ^{7}Li-induced reactions.

The overlap between bands of identified $\alpha + p$ (red) and $\alpha + d$ (magenta) for ^{6}Li-induced reactions, as seen in Fig. 3, means that for mass-unidentified coincidences, separation of the $\alpha + d$ and $\alpha + p$ contribution is nontrivial. The separation of these two contributions requires the reconstruction of the three-body reaction Q value to precisely determine the particles species involved, and thus the reaction process. This Q-value reconstruction process also allows the verification of the origin of the $\alpha + \alpha$ coincidences, as described below.

III. MECHANISMS OF BREAKUP

To identify and understand the processes taking place during the reaction, it is important to determine the energy change (Q value) associated with each event. Consider a two-body collision with a projectile having initial and final kinetic energy E_{lab} and E_{f}, respectively. The ground-state Q value, Q_{gg}, for any collision can be written as

$$Q_{\mathrm{gg}} = E_{\mathrm{f}} + E_{\mathrm{ex,PL}} + E_{\mathrm{ex,TL}} + E_{\mathrm{rec}} - E_{\mathrm{lab}}, \tag{1}$$

where E_{f} is the kinetic energy of the projectile-like nuclei, $E_{\mathrm{ex,PL}}$ and $E_{\mathrm{ex,TL}}$ are the excitation energies of the projectile-like and target-like nuclei, respectively, and E_{rec} is the recoil energy of the latter, all in the laboratory frame.

Usually, the excitation energies of the projectile-like and target-like nuclei are not measured at the same time as the kinetic energies. However, if the projectile-like nucleus breaks up, its excitation energy $E_{\mathrm{ex,PL}}$ is shared by the kinetic energies E_i of the fragments. Thus for binary breakup, $E_{\mathrm{f}} + E_{\mathrm{ex,PL}} = E_1 + E_2$. Since the reaction Q value is related to Q_{gg} by $Q = Q_{\mathrm{gg}} - E_{\mathrm{ex,TL}}$, therefore Eq. (1) can be written as

$$Q = E_1 + E_2 + E_{\mathrm{rec}} - E_{\mathrm{lab}}, \tag{2}$$

where E_{lab} is derived from E_{beam} after correcting for energy lost in traversing the target. The recoil energy E_{rec} is not measured, but through conservation of momentum, can be calculated knowing the momenta and masses of the two detected fragments, and assuming no additional undetected particle was produced during the reaction. If a fourth particle were produced, its kinetic energy would perturb the Q value much more than its effect on calculating E_{rec}, which for the reactions studied here, is typically 3 to 4 MeV. The excitation energy $E_{\mathrm{ex,TL}}$ of the target-like nucleus cannot be captured in our detector, the Q spectra will show separate peaks for each state populated in the target-like nucleus.

Only events with correlated energies which lie inside the E_1 vs. E_2 gates shown in Fig. 3 are considered for Q-values calculation. For mass-identified coincident events, the $\alpha + t$, $\alpha + d$ and $\alpha + p$ modes can be clearly identified, and thus their Q-value assignment is unambiguous. The Q spectra for each mass-identified breakup mode allows identification of breakup modes for mass-unidentified coincidence events as discussed briefly next.

In the event-by-event data analysis, for each mass-unidentified coincidence, four Q values were determined assuming four possible breakup modes namely $\alpha + \alpha$, $\alpha + t$, $\alpha + d$, and $\alpha + p$. In determining E_{rec}, the higher kinetic energy of $E_{1,2}$ was assigned to the α particle, and the other assigned to an α particle, triton, deuteron, and proton successively. The event is then considered to belong to a particular breakup channel if the resultant $Q_{\alpha+x}$ matches that of the mass-identified $Q_{\alpha+x_{\mathrm{ID}}}$ peak for the respective breakup channel. In the few cases where the $Q_{\alpha+x}$ is consistent with peaks of more than one breakup mode in the mass-identified Q spectra, event-by-event assignment is not possible. Here the Q-spectrum decomposition was performed, as described in the Appendix.

Shown in Fig. 4 are the reconstructed Q spectra for the reactions of ^{7}Li with ^{144}Sm at $E_{\mathrm{beam}} = 24.0$ MeV and ^{6,7}Li with ^{207,208}Pb and ^{209}Bi at $E_{\mathrm{beam}} = 29.0$ MeV. These energies are close to the respective barrier energies for each reaction. In common with results at all measured energies, these spectra show that almost all the yield contributes to sharp peaks in Q, meaning the breakup is indeed almost exclusively binary, with identified breakup modes of $\alpha + \alpha$ (green), $\alpha + t$ (blue), $\alpha + d$ (magenta), and $\alpha + p$ (red). Peaks in the Q spectra can be seen to have a FWHM ≈0.20 MeV. The expected Q_{gg} for all binary breakup modes are indicated by vertical dashed lines from the axis. The good agreement of the most positive peak for each mode with expectations demonstrates the effectiveness of the calibration of the detector array.

A. Breakup modes for ^{7}Li

In reactions of ^{7}Li, breakup into $\alpha + t$ is prominent, with the experimental Q value centered at the expected Q_{gg} [Fig. 4(a)–4(d)]. However, the production of ^{8}Be, through p-pickup, which subsequently breaks up into two α particles, is more probable. Peaks in the Q spectra corresponding to $\alpha + \alpha$ breakup show that the target-like products ^{143}Pm, ^{206,207}Tl and ^{208}Pb are populated mostly in their excited states. The $\alpha + d$ breakup mode, triggered by n stripping of ^{7}Li forming excited ^{6}Li, is also present and is noticeably more prominent than $\alpha + t$ breakup for the ^{207}Pb target. The $2n$-stripping reactions, forming the unbound ^{5}Li, results in the observed $\alpha + p$ products. The α particles from all three transfer-triggered breakup modes do not have a corresponding triton, which helps explain the one order of magnitude higher inclusive cross sections for α particles than tritons observed [37] for the reaction of ^{7}Li with ^{208}Pb.

For the reaction of ^{7}Li with ^{144}Sm [Fig. 4(a)], the Q-value peak for $\alpha + t$ breakup overlaps with that of $\alpha + d$ breakup after n stripping, where the target-like nuclei are populated in excited states. Cross-contamination between $\alpha + t$ and $\alpha + d$ coincidence yield is thus possible during the separation of mass-unidentified events. The yield for $\alpha + p$ breakup, through $2n$ stripping, is particularly prominent for this target. This yield is in effect underestimated as the Q values for mass-unidentified $\alpha + p$ events overlap with those for $\alpha + t$ and $\alpha + d$ breakup. It should be mentioned that there was no ambiguity in the separation of $\alpha + p$ breakup from $\alpha + \alpha$, even though $Q_{\alpha+p}$ and $Q_{\alpha+\alpha}$ can be seen overlapping. This is because those $\alpha + p$ coincidences with E_p vs. E_α overlapping with E_α vs. E_α from $\alpha + \alpha$ coincidences all have the proton with high energy and thus are identified by ΔE-E telescope, as seen in Fig. 3.

For the reaction of ^{7}Li with ^{209}Bi, the Q spectra for $\alpha + \alpha$ breakup (triggered by p pickup) is remarkably similar to that for the reaction of ^{7}Li with ^{208}Pb, except with three additional peaks at higher Q values. This is a manifestation of nuclear shell structures where similarity between the structure of ^{208}Pb and ^{209}Bi results in similar $Q_{\alpha+\alpha}$ spectra, and the unpaired proton in ^{209}Bi results in the three additional peaks in $Q_{\alpha+\alpha}$, seen only for this target.

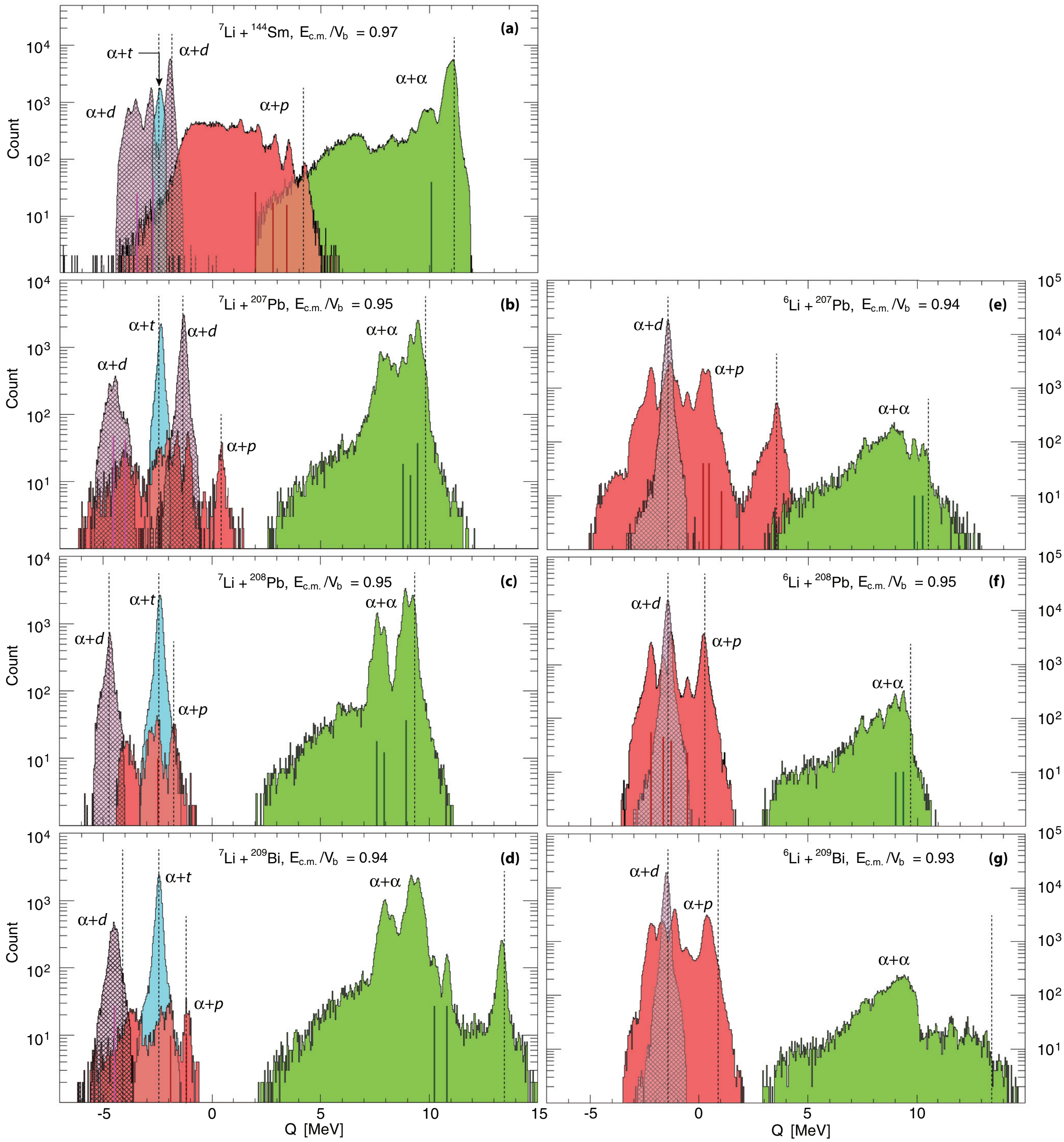

FIG. 4. (Color online) Q spectra determined for the reaction of ^{7}Li with ^{144}Sm at $E_{\text{beam}} = 24.0$ MeV and ^{6,7}Li with ^{207,208}Pb and ^{209}Bi at $E_{\text{beam}} = 29.0$ MeV. Identified breakup modes consist of $\alpha + p$ (red), $\alpha + d$ (magenta with hatching), and $\alpha + \alpha$ (green). Dashed lines indicate the expected Q_{gg} for each breakup mode. The vertical lines, in a darker shade of the color of the respective breakup mode, indicate Q values for breakup following the population of known excited states of the target-like nucleus. Peaks in the Q spectra without corresponding vertical lines include breakup following the population of excited states of the target-like nuclei where the separation in energy of the excited states is much smaller than the width of the peaks and thus they cannot be identified reliably. These spectra appear cleaner than expected from the E_1 vs. E_2 plots (Fig. 3) because they include only events with correlated energies inside the polygons shown in Fig. 3.

B. Breakup modes for ^{6}Li

For binary breakup in reactions of ^{6}Li [Fig. 4(e)–4(g)], the most intense peak, at all bombarding energies, coincides with the Q value for breakup of the projectile into its $\alpha + d$ cluster constituents. Breakup triggered by nucleon(s) transfer is also highly probable for ^{6}Li. Breakup into $\alpha + p$ contributes multiple distinct peaks in the spectrum. The peak with the highest Q in most cases is centered at Q_{gg} for $\alpha + p$ breakup, matching the expected Q values for n-stripping from the projectile and forming the unbound ^{5}Li. Breakup of ^{8}Be into $\alpha + \alpha$, triggered by d pickup, is also observed for ^{6}Li. The prominence of breakup triggered by nucleon(s) transfer also helps to explain why unusually large numbers of α particles, compared to deuterons, were observed [41,42] in previous measurements for ^{6}Li.

As shown in the Appendix, separating the yields of $\alpha + p$ and $\alpha + d$ coincidences from mass-unidentified events is not straight forward and required intricate gates and judgment based on the general trend of groups of events. Some cross-contamination between the yields for the $\alpha + d$ and $\alpha + p$ breakup mode is highly probable for ^{6}Li, despite the best efforts in the analysis process.

IV. TIME-SCALES OF BREAKUP

Identification of the reaction processes leading ultimately to breakup of the projectile-like nucleus, while important for understanding reaction mechanisms, is not sufficient to understand the interplay between breakup and suppression of CF. It is critical to also know the time-scale [27] of each process, i.e., whether these nuclei would have arrived at the barrier radius and undergo CF, in collisions at above-barrier energies. For example, although formation of ^{8}Be (through p pickup by ^{7}Li at sub-barrier energies) can only occur close to the target nucleus, its ground-state lifetime [36] is long: $\sim 10^{-16}$ s. At sub-barrier energies, the ^{8}Be nucleus will not have enough energy to fuse with the target-like nucleus. The eventual ground-state decay into two α particles may happen in the asymptotic region, after ^{8}Be has receded many thousands of nuclear diameters from the target-like nucleus. This probability for *asymptotic* breakup at sub-barrier energies can be extrapolated to collisions at above-barrier energies. However, this asymptotic breakup can have no effect on CF at above-barrier energies as all ^{8}Be populated in the long-lived ground state would arrive intact at the barrier radius to contribute to CF. Only ^{8}Be populated in excited states, having much shorter ($< 0.5 \times 10^{-22}$ s) lifetimes [36], may compete with CF though *prompt breakup* which depletes the flux of intact nuclei before the fusion barrier is reached. The Q-value spectra give no clue to the relative population between the ground and excited states of ^{8}Be. However, the energy $E_{\mathrm{ex,PL}}$ of the excited states of ^{8}Be appears in the kinetic energies $E_{1,2}$ of the breakup fragments, and have been shown [27] to be related to the time-scales of the process. Similar observation has also been made in the breakup of ^{9}Be [26,28].

For asymptotic breakup on the outgoing trajectory, the energy of the fragments in the reference frame of the projectile-like nucleus (the relative energy E_{rel}) is given by the sum $Q_{\mathrm{BU}} + E_{\mathrm{ex,PL}}$ [27,43], where Q_{BU} is the breakup Q value. The relative energy can be expressed in terms of the measured energies E_i and deduced masses m_i, and the measured angular separation θ_{12} of the fragments

$$E_{\mathrm{rel}} = \frac{m_2 E_1 + m_1 E_2 - 2\sqrt{m_1 E_1 m_2 E_2}\cos\theta_{12}}{m_1 + m_2}. \qquad (3)$$

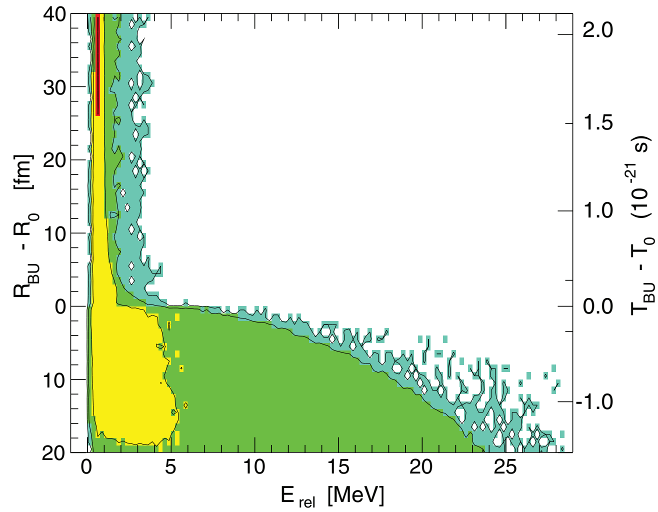

FIG. 5. (Color online) Landscapes of the classically calculated E_{rel} versus the nuclear separation (left axis) or time (right axis) at which $^6\mathrm{Li} \to \alpha + d$ breakup occurs, relative to the point of closest approach (R_0, T_0) for ^{6}Li in the field of a ^{207}Pb nucleus. The spread in E_{rel} arises from the different impact parameters and fragments orientations at the moment of breakup. Breakup prior to reflection, $(T_{\mathrm{BU}} - T_0) < 0$ results in higher E_{rel} values than breakup after reflection $(T_{\mathrm{BU}} - T_0) > 0$. Impact parameters corresponding to angular momenta up to $49\hbar$ were considered. (Contour lines correspond to one order of magnitude in yield.)

However, for breakup close to the target nucleus, the fragment trajectories are perturbed by its presence, and E_{rel} no longer depends solely on the breakup energetics. The quantitative dependence of E_{rel} on the internuclear separation at breakup can be determined classically using a three-body three dimensional model such as PLATYPUS [29–31].

A. Relating breakup time-scales to the relative energy of the breakup fragments

An illustrative calculation of the dependence of E_{rel} on the projectile-target separation at which breakup occurs (R_{BU}) was performed for breakup of ^{6}Li from the 3^+ (2.186 MeV, lifetime 2.7×10^{-20} s) state using the aforementioned code PLATYPUS. For this illustration, the distance R_{BU} was *uniformly* sampled along the trajectory of the ^{6}Li projectile, having energy $E_{\mathrm{beam}} = 29.0$ MeV. The orientations of the $\alpha + d$ fragments at R_{BU}, relative to the target nucleus, were also randomly sampled with an isotropic distribution. The result of this calculation is shown in Fig. 5. Since this is a classical calculation, the time of breakup T_{BU} relative to that of the closest approach (T_0) could be exactly evaluated, and is also shown. For comparison, the one-dimensional experimental E_{rel} spectra for $\alpha + d$ coincidences, from breakup of ^{6}Li on ^{207}Pb at $E_{\mathrm{beam}} = 29.0$ MeV, is shown above in magenta.

The dependence of E_{rel} on R_{BU}, relative to the point of closest approach without breakup (R_0), can be seen through the variation of E_{rel} as a function of $R_{\mathrm{BU}} - R_0$. The wide spread of E_{rel} from breakup before reaching R_0 indicates that breakup that can suppress CF will be characterised by a broad E_{rel}

distribution due to post-breakup acceleration of the fragments in the Coulomb field of the target nucleus. For asymptotic breakup after the projectile-like nucleus has traveled past R_0, the relative energy E_{rel} asymptotically approach $\approx$0.7 MeV, the energy available at breakup ($Q_{\text{BU}} + E_{\text{ex,PL}}$). All features in the simulated E_{rel} vs. R_{BU} are consistent with both the peak and the broad E_{rel} component in the experimental E_{rel} spectrum [see Fig. 7(b)].

The mapping of radius R_{BU} to the breakup time T_{BU} allows correlation of the time-scale for breakup to the measured E_{rel}. Given that transfer occurs on time-scales of $\sim 10^{-22}$ s [27], information on T_{BU} allows the classification of breakup into *prompt* ($T_{\text{BU}} \approx$ a few 10^{-22} s), or *delayed* breakup. Prompt breakup results in breakup of the projectile or projectile-like nuclei on the entrance trajectory, and thus reduces the flux of intact nuclei available for fusion at the distance of closest approach R_0. On the other hand, delayed breakup happens on the exit trajectory, in the asymptotic region. These nuclei have survived breakup and are intact at R_0, and thus are able to participate in fusion if the beam energy is above the barrier.

It is important at this point to reiterate the clear distinction between the locations (and times) of the process *triggering* breakup and the subsequent breakup; e.g., the formation of ^{8}Be through p pickup by ^{7}Li, and the subsequent breakup of ^{8}Be into $\alpha + \alpha$. Breakup can follow promptly after the creation of ^{8}Be and results in a high E_{rel}, or can happen in the asymptotic region far from the target with low E_{rel}. Thus, the experimental E_{rel} gives us a measure of the location at which the breakup fragments are produced. It is therefore not a measure of the location of the process triggering breakup.

It has been predicted theoretically [29], and observed experimentally [23,26], that at energies below the barrier the probability of breakup is well described by an exponential dependence on inter-nuclear separation. For the $\alpha + \alpha$ breakup triggered by p pickup by ^{7}Li, the exponential slope was determined from our measurements of the probabilities as a function of beam energy. Along a projectile trajectory, the transfer probability was found to be strongly peaked around R_0, with 50% of the yield occurring within $|R_{\text{BU}} - R_0| <$ 0.7 fm, and 95% within $|R_{\text{BU}} - R_0| <$ 2.7 fm. These correspond to times of $\pm 1.5 \times 10^{-22}$ s and $\pm 4.5 \times 10^{-22}$ s around the time of closest approach T_0. For fusion of ^{7}Li to be suppressed by means of formation of ^{8}Be, $\alpha + \alpha$ breakup of ^{8}Be must occur before the projectile passes R_0, i.e., before ^{8}Be starts receding from the target-like nucleus. This gives a qualitative indication of the short delay between transfer and breakup that is allowable if transfer-triggered breakup is to affect CF.

B. Correlation of Q value and E_{rel}

Shown in Fig. 6 are the measured Q vs. E_{rel} two-dimensional spectra for a selection of measurements for the reactions of ^{7}Li with ^{144}Sm and ^{6,7}Li with ^{207,208}Pb and ^{209}Bi. Genuine breakup events are shown in colors, with the $\alpha + \alpha$ breakup mode in green, $\alpha + t$ in blue, $\alpha + d$ in magenta, and $\alpha + p$ in red. For each reaction studied, the same reaction channels were observed at all energies measured as shown in Fig. 6(a)–6(c) for the reaction of ^{7}Li with ^{207}Pb.

From the established relationship between the E_{rel} spectrum and the time-scale of breakup (Fig. 5), the Q vs. E_{rel} spectra shown in Fig. 6 thus contain a *complete* picture of breakup modes in the reactions of ^{6,7}Li. For each breakup event, its Q value defines the breakup mode, revealing the reaction process triggering breakup, and also the excitation of the target-like nucleus. At the same time, the determination of E_{rel} gives the information on the time-scale of the binary breakup which, in turn, allows a degree of separation between *prompt* and *asymptotic* breakup.

The same breakup mode can originate from different projectile-target combinations and/or different preceding processes (e.g., direct breakup or transfer leading to breakup). Figure 6 shows that qualitatively they share the same E_{rel} features. For example, the breakup of $^6\text{Li} \rightarrow \alpha + d$ following either n stripping from ^{7}Li [Fig. 6(a)–6(f)] or direct breakup of ^{6}Li [Fig. 6(g)–6(i)], all have the same high concentration of events with $E_{\text{rel}} = 0.7$ MeV and a broad tail leading to higher E_{rel}. The $^8\text{Be} \rightarrow \alpha + \alpha$ breakup, following both p pickup by ^{7}Li and d pickup by ^{6}Li, all have a high intensity of events with $E_{\text{rel}} \approx 0.1$ MeV and broad tails comprising high E_{rel} events. This follows qualitatively the behavior of asymptotic and prompt breakup, respectively, as expected from the classical model calculations (Fig. 5).

C. Interpretation of E_{rel} spectra

More subtle differences between the E_{rel} distributions, especially the relative population of prompt and delayed breakup, emerges upon closer inspection of the E_{rel} spectra. Shown in Fig. 7 are E_{rel} spectra for all major breakup modes identified from the reactions of ^{7}Li with ^{144}Sm at $E_{\text{beam}} =$ 24.0 MeV, and ^{6,7}Li with ^{207,208}Pb and ^{209}Bi at $E_{\text{beam}} =$ 29.0 MeV. These spectra have been corrected for loss of events with incomplete energy deposition, and detection efficiency with respect to E_{rel}, for each individual breakup mode. The method for determining the efficiency of the detector array for the detection of all breakup events occurring at a given beam energy is described in Ref. [26] for the $\alpha + \alpha$ breakup mode. This method was applied for all other breakup modes by using the appropriate interaction potentials and measured breakup probabilities. The efficiency varies as a function of the relative energy of the coincidence particles as shown in Ref. [27]. It also depends on the breakup mode, for example at $E_{\text{rel}} = 5$ MeV it ranges from $\sim$5% for $\alpha + d$ to $\sim$15% for $\alpha + \alpha$.

1. Instrumental E_{rel} resolution

For breakup far from the target nucleus, the relative energy of the two fragments is exactly equal to the energy available at breakup (i.e., $Q_{\text{BU}} + E_{\text{ex,PL}}$). However, instrumental effects of finite energy resolution of the DSSDs and the pixel size lead to a spread in E_{rel}, which can be calculated easily using Monte Carlo simulations as detailed in Ref. [26]. These were done to calculate the detector response for $^8\text{Be}_{\text{g.s.}} \rightarrow \alpha + \alpha$ (lifetime $\sim 10^{-16}$ s) with 92 keV of available breakup energy, and $^6\text{Li} \rightarrow \alpha + d$ from the 3^+ excited state (lifetime $\sim 2.7 \times 10^{-20}$ s) with available energy of 0.71 MeV. The nuclei ^{5}Li and ^{7}Li do

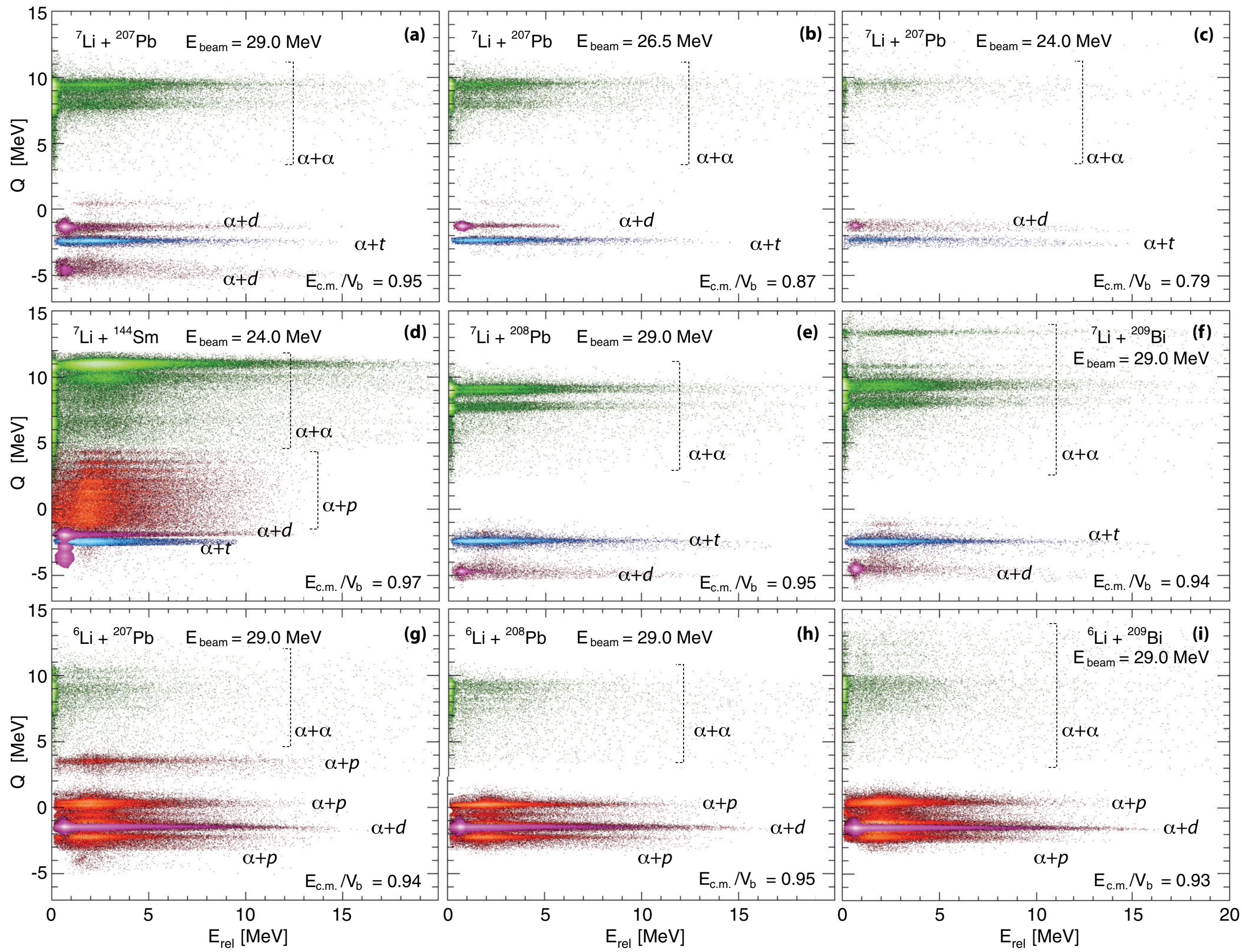

FIG. 6. (Color online) Scatterplots of Q value vs. $E_{\rm rel}$ for the indicated reactions. Colored regions show the identified genuine breakup events belonging to the $\alpha + \alpha$ (green), $\alpha + t$ (blue), $\alpha + d$ (magenta), and $\alpha + p$ (red) breakup modes. These spectra have neither been corrected for events with incomplete energy deposition, nor for geometrical efficiency. The paler shade for each breakup mode corresponds to higher intensity.

not have long-lived states (lifetimes $>10^{-20}$ s). Nevertheless to demonstrate that the broad features in $E_{\rm rel}$ in Fig. 7(c) and Fig. 7(d) are not the effect of instrumental resolution, calculation were done for ^{7}Li $\rightarrow \alpha + t$ with available energy of 2.18 MeV (notionally corresponding to breakup from the $\frac{7}{2}^-$ excited state) and ^{5}Li $\rightarrow \alpha + p$ with available energy of 1.96 MeV. The calculated detector responses are shown in Fig. 7 by the shaded peaks. The calculations match extremely well with the experimentally observed peak centered at 92 keV in panel (a) corresponding to ^{8}Be$_{\rm g.s.} \rightarrow \alpha + \alpha$ and the peak centered at 0.7 MeV in panel (b) due to ^{6}Li $\rightarrow \alpha + d$. The good match between the calculated width and that observed experimentally demonstrates that the widths of the narrow peaks in (a) and (b) indeed arise from instrumental resolution. The experimental data in panels (c) and (d) do not show narrow peaks, indicating that prompt breakup of ^{5}Li and ^{7}Li (in close proximity to the heavy target nucleus) is predominant. The decay modes shown in each panel are discussed in detail below.

2. Features of experimental E_{rel} spectra

For both ^{6}Li- and ^{7}Li-induced reactions, the experimental $E_{\rm rel}$ spectra for ^{8}Be $\rightarrow \alpha + \alpha$ breakup [Fig. 7(a)] show a sharp peak at 92 keV, which as discussed in Sec. IV C1, corresponds to the ground-state decay of ^{8}Be in the asymptotic region far from the target. The area under this peak of ground-state decay of ^{8}Be comprises $\approx$40% of all the $\alpha + \alpha$ yield in the reactions of ^{6,7}Li with ^{207,208}Pb and ^{209}Bi. For the reaction of ^{7}Li with ^{144}Sm, however, the ground-state decay of ^{8}Be contributes to only $\approx$10% of the total $\alpha + \alpha$ yield. The majority of $\alpha + \alpha$ breakup is prompt, as emphasised by the broad bump with $E_{\rm rel} > 0.5$ MeV.

For the ^{6}Li $\rightarrow \alpha + d$ breakup [Fig. 7(b)], the sharp peak at 0.7 MeV in the $E_{\rm rel}$ spectra corresponds to the decay of the 3^+ state of ^{6}Li. This state is populated either through direct excitation of ^{6}Li, or through n stripping of ^{7}Li. For breakup following direct excitation of ^{6}Li, $\approx$35% of the total $\alpha + d$ yield has $E_{\rm rel}$ ~0.7 MeV, indicating these breakup events occur

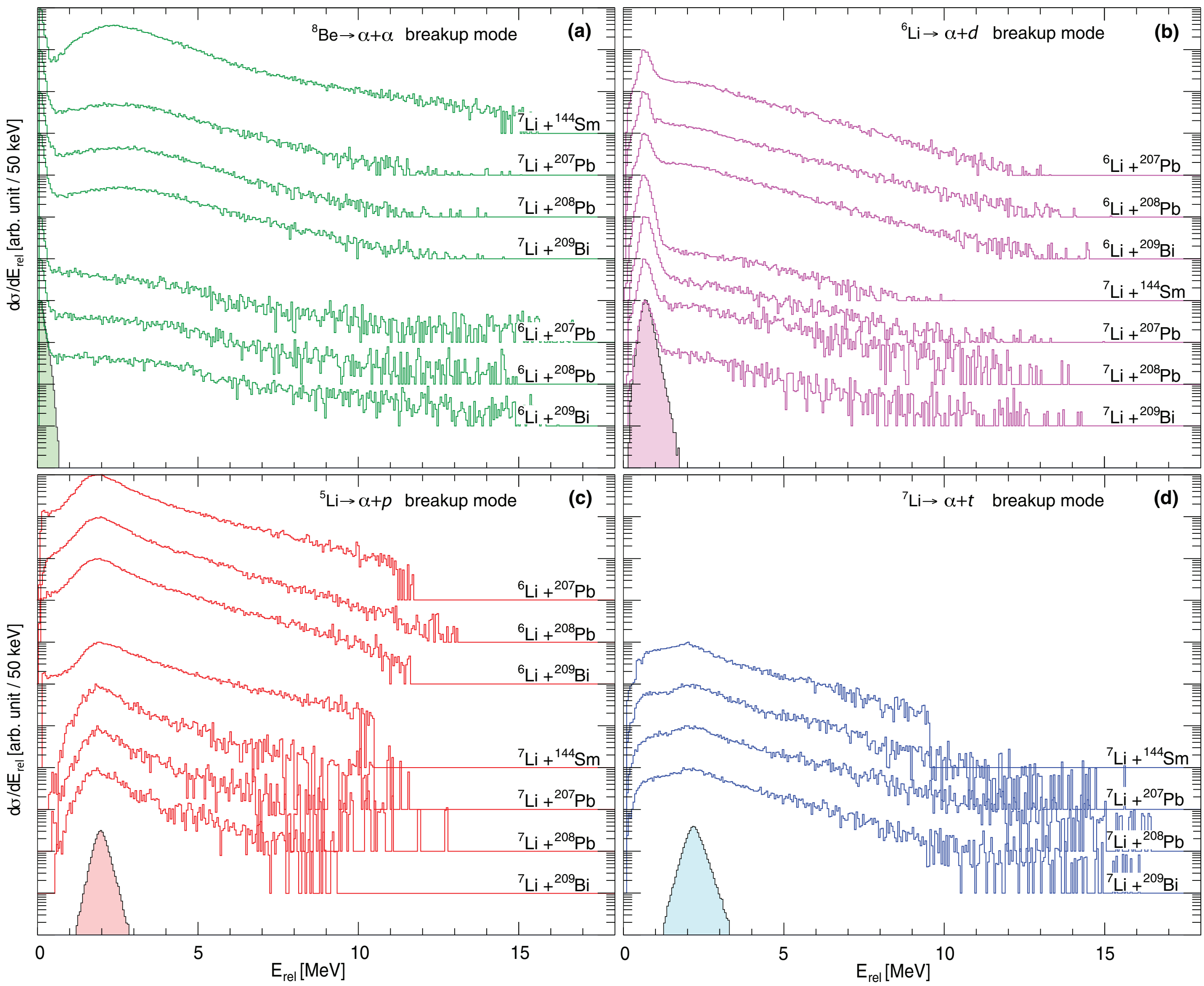

FIG. 7. (Color online) $E_{\rm rel}$ spectra, corrected for events with incomplete energy deposition and detector efficiency, for identified breakup partitions are plotted in bins of 50 keV for the indicated reactions. Spectra are plotted up to values of $E_{\rm rel}$ where the counts reach a level of 10^{-3} of the maximum yield. The instrumental resolution for each breakup channel is indicated by the shaded peaks, calculated for representative Q values in each case (see text).

in the asymptotic region. For breakup following n stripping of ^{7}Li, the population of breakup with low $E_{\rm rel}$ is higher than seen for direct breakup of ^{6}Li, and variable, being ≈55% for ^{209}Bi, ≈45% for ^{208}Pb, ≈75% for ^{207}Pb, and ≈75% for ^{144}Sm. This indicates that ^{6}Li formed though n-stripping is likely to be formed at low excitation energies, probably due to the lower available energy resulting from the negative Q value associated with n stripping. The shaded peak confirms that the observed width (FWHM ∼0.3 MeV) of the 0.7 MeV peak is an instrumental effect of the detector pixel size.

We now consider only breakup processes contributing to a broad $E_{\rm rel}$ distribution. All $^5{\rm Li} \rightarrow \alpha + p$ breakup $E_{\rm rel}$ spectra measured [Fig. 7(c)] have predominantly high $E_{\rm rel}$. This mode makes the largest contribution to the overall prompt breakup in reactions of ^{6}Li. This breakup mode also makes a significant contribution to the prompt breakup, through $2n$ stripping, in the reaction of ^{7}Li with ^{144}Sm.

For the direct $^7{\rm Li} \rightarrow \alpha + t$ breakup [Fig. 7(d)], the broad distribution to high $E_{\rm rel}$ shows its largely prompt nature. All $E_{\rm rel}$ spectra for $\alpha + t$ breakup shows a slight peak at $E_{\rm rel}$ ∼2.1 MeV, perhaps due to a tiny fraction of breakup from the $\frac{7}{2}^-$ (4.65 MeV) state of ^{7}Li as predicted [44] using a dicluster $\alpha + t$ model. This state has a lifetime of $\sim 9 \times 10^{-21}$ s which might just be long enough to see the projectile breakup in the asymptotic region. The shaded peak shows the calculated width, due to instrumental effects, that is expected for breakup of this state in the asymptotic region.

V. RELATIVE PROBABILITIES FOR PROMPT BREAKUP

Breakup events in reactions of ^{6,7}Li arise either though direct excitation of ^{6,7}Li or through formation of intermediate nuclei via nucleon transfer which then undergo breakup.

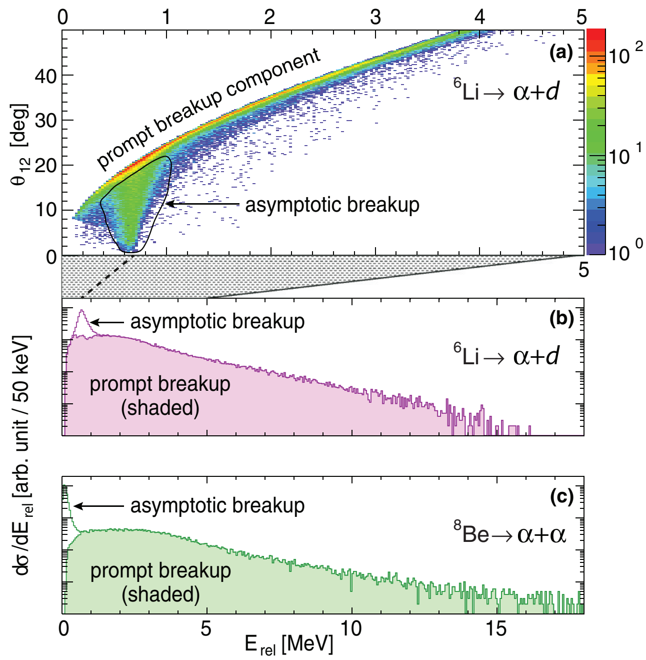

FIG. 8. (Color online) (a) Experimental θ_{12} vs. $E_{\rm rel}$ scatterplot from the reaction of ^{6}Li with ^{209}Bi at $E_{\rm beam} = 29.0$ MeV. The correlation between θ_{12} and $E_{\rm rel}$ is distinctly different between prompt (the main feature) and asymptotic breakups (enclosed region). (b,c) Separation of prompt $\alpha + d$ and $\alpha + \alpha$ breakup components from their respective total breakup yields, based on the correlation between the experimental θ_{12} and $E_{\rm rel}$. The sample spectra shown are from the reactions of ^{6,7}Li with ^{209}Bi at $E_{\rm beam} = 29.0$ MeV, respectively.

Whatever the breakup mechanism, only the prompt breakup components can suppress complete fusion for energies at and above the barrier.

To determine the total prompt breakup in reactions of ^{6,7}Li, the prompt breakup components for the $\alpha + d$ and $\alpha + \alpha$ breakup modes have been separated from the delayed (asymptotic) breakup. This was done by subtraction of the estimated contribution from asymptotic breakup components [the narrow peaks in the experimental $E_{\rm rel}$ spectra seen in Fig. 7(a) and Fig. 7(b)]. The procedure to estimate the asymptotic breakup component is illustrated in Fig. 8(a), which shows the θ_{12} vs. $E_{\rm rel}$ scatterplot for $\alpha + d$ coincidence from the reaction of ^{6}Li + ^{209}Bi at $E_{\rm beam} = 29.0$ MeV. The correlation between the θ_{12} and $E_{\rm rel}$ are distinctly different for prompt (the intense band) and asymptotic breakup (enclosed region). This allowed their separation as shown in Fig. 8(b). The prompt $\alpha + \alpha$ breakup was similarly separated from the total $E_{\rm rel}$ spectra as shown in Fig. 8(c) for the reaction of ^{7}Li with ^{209}Bi at $E_{\rm beam} = 29.0$ MeV. This separation method has been applied to all $\alpha + d$ and $\alpha + \alpha$ spectra.

Shown in Fig. 9 are the relative contributions (efficiency corrected) to prompt breakup by all the major identified breakup modes. Prompt direct breakup into the projectile cluster constituents dominates at $E_{\rm c.m.}/V_{\rm b} \lesssim 0.87$ for both ^{6}Li and ^{7}Li, except for the reaction of ^{7}Li with ^{144}Sm. At energies closer to the barrier, prompt breakup triggered by transfer dominates.

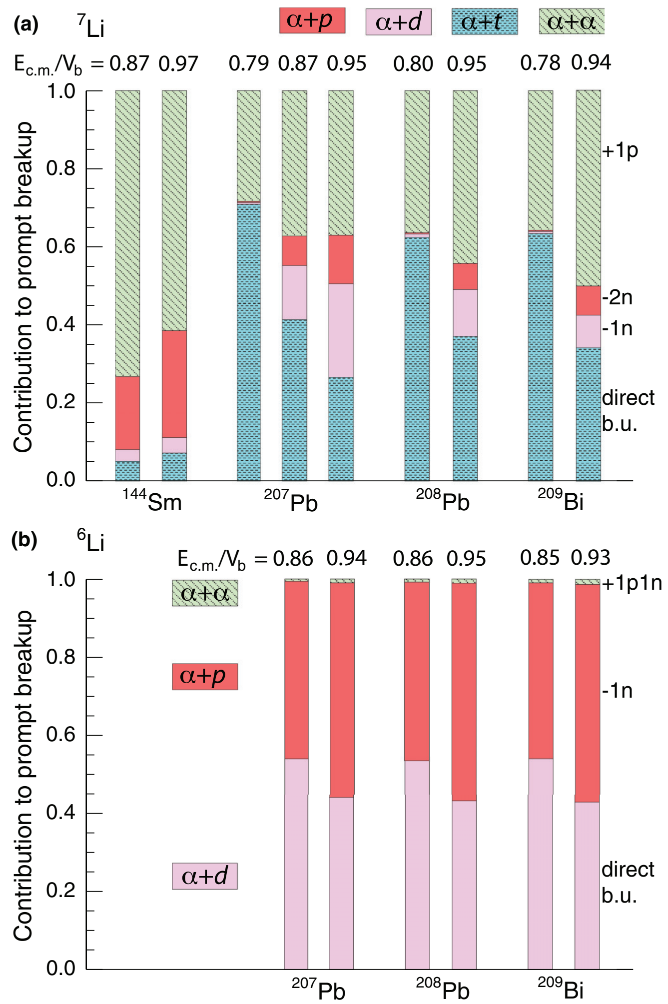

FIG. 9. (Color online) Relative contribution by the prompt $\alpha + \alpha$, $\alpha + t$, $\alpha + d$, and $\alpha + p$ breakup to the total prompt breakup of ^{6,7}Li on indicated targets. The fractional contribution from the prompt $\alpha + d$ and $\alpha + p$ breakups to the total prompt breakup of ^{6}Li is very similar, but not identical, across all three targets.

For the ^{7}Li-induced reactions [Fig. 9(a)], the largest contribution to prompt breakup is triggered by p pickup, resulting in the prompt $\alpha + \alpha$ breakup of the ^{8}Be projectile-like nuclei. Breakup triggered by n stripping also plays a role in reactions with ^{7}Li. Of interest is the large contribution from $\alpha + p$ breakup, triggered by $2n$ stripping, for the reaction of ^{7}Li with ^{144}Sm. It is about three times the total contribution from prompt $\alpha + d$ and $\alpha + t$ breakup. This large contribution of $2n$ stripping may be due to the positive (+2.250 MeV) Q value associated with this transfer reaction. In contrast the Q values for $2n$ stripping are negative for all other targets studied here. Further investigation and contrast with the more deformed ^{154}Sm, or moving to reactions with much lighter targets, would reveal any systematics behind this behavior. For the reactions with ^{6}Li [Fig. 9(b)], the predominance of breakup triggered by n stripping (^{6}Li → ^{5}Li → $\alpha + p$) over direct cluster breakup (^{6}Li → $\alpha + d$) is rather target independent, as similar results were observed on all three targets ^{207}Pb, ^{208}Pb and ^{209}Bi.

The predominance of breakup triggered by transfer, at sub-barrier energies, may play an important role in explaining the observed [6,7,45–47] above-barrier suppression of CF for both ^{6}Li and ^{7}Li. The extraction of *absolute* prompt breakup probabilities as a function of beam energy is in progress, and will allow quantitative estimation of the amount of complete fusion suppression, due to breakup of the projectile or projectile-like nuclei, at above-barrier energies.

VI. CONCLUSION

The measurements presented in this work carry the most complete information on breakup modes in reactions of the weakly bound stable nuclei ^{6,7}Li with heavy targets. Breakup with both ^{6}Li and ^{7}Li projectiles is found to be triggered predominantly by nucleon transfer, n stripping for ^{6}Li, and p pickup for ^{7}Li. The dominance of transfer-initiated breakup for both ^{6}Li and ^{7}Li, with resultant breakup fragments being different from the initial mass-partition, will be a major challenge for the quantum theory of low energy nuclear reactions. From the relative energy E_{rel} of the binary breakup fragments, information on the breakup time-scales allows the separation of prompt and asymptotic breakup components. To facilitate the understanding and development of a theoretical framework for predicting these reactions, and the prediction of the effect of breakup on complete fusion at above-barrier energies, the determination of absolute probabilities from these prompt breakup results is currently being pursued, and will be described in a forthcoming paper.

ACKNOWLEDGMENTS

The authors are grateful for the exceptional contributions of N. Lobanov, A. Muirhead, and D. Tsifakis, as well as all the accelerator staff of the ANU Heavy Ion Accelerator Facility. The authors acknowledge support from the Australian Research Council, through Discovery Grants No. DP110102879, No. DP130101569 and Program No. FL110100098.

APPENDIX: DETERMINING THE BREAKUP MODE FOR MASS-UNIDENTIFIED EVENTS

As an illustration, the steps in determining $\alpha + d$ and $\alpha + p$ breakup from mass-unidentified events for the reaction of ^{7}Li with ^{207}Pb at $E_{\mathrm{beam}} = 29.0$ MeV are shown in Fig. 10. The pale shaded spectrum in Fig. 10(a) shows the calculated Q spectrum assuming an $\alpha + d$ breakup mode for the mass-unidentified events. One peak in $Q_{\alpha+\mathrm{d}}$ is seen to be aligned with the peak in $Q_{\alpha+d_{\mathrm{ID}}}$, identified as $\alpha + d$ breakup by the ΔE-E telescope. Events under this peak in $Q_{\alpha+\mathrm{d}}$, shown by hatching, are assigned as $\alpha + d$ breakup events. Similarly, the pale shaded spectrum in Fig. 10(b) is the calculated $Q_{\alpha+\mathrm{p}}$ spectrum for mass-unidentified events. Events that form peaks which align with peaks in the $Q_{\alpha+p_{\mathrm{ID}}}$ spectra of known $\alpha + p$ breakup are assigned as genuine $\alpha + p$ breakup events.

For cases where peaks in $Q_{\alpha+d}$ and $Q_{\alpha+p}$ overlap, these peaks comprise two contributions; one due to breakup into the $\alpha + d$ partition and the other from the $\alpha + p$ breakup mode. An isolated peak is identified in the measured $Q_{\alpha+\mathrm{pID}}$ spectrum together with its corresponding peak in the $Q_{\alpha+\mathrm{p}}$ spectrum

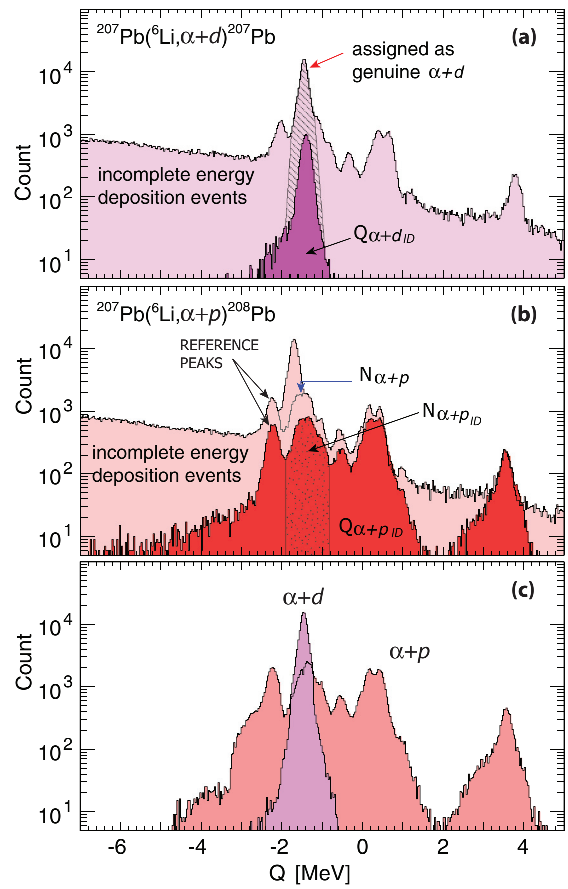

FIG. 10. (Color online) Determination of breakup modes for binary events from the reaction ^{6}Li with ^{207}Pb at $E_{\mathrm{beam}} = 29.0$ MeV. In pale colors are Q spectra for mass-unidentified coincidence events, calculated assuming (a) $\alpha + d$ breakup and (b) $\alpha + p$ breakup. The overlaid (dark colors) in (a) and (b) are Q spectra for events with an identified deuteron $Q_{\alpha+d_{\mathrm{ID}}}$ or proton $Q_{\alpha+p_{\mathrm{ID}}}$ respectively. Alignment of a peak in $Q_{\alpha+\mathrm{d}}$ with $Q_{\alpha+d_{\mathrm{ID}}}$ identifies events under this peak in $Q_{\alpha+\mathrm{d}}$ as genuine $\alpha + d$ breakup in (a). Alignment of peaks in $Q_{\alpha+\mathrm{p}}$ with $Q_{\alpha+p_{\mathrm{ID}}}$ identifies events under those peaks in $Q_{\alpha+\mathrm{p}}$, in (b), as genuine $\alpha + p$ breakup. (c) Final Q spectra showing contribution from $\alpha + d$ and $\alpha + p$ breakup.

[labeled as reference peaks in Fig. 10(b)]. The raw counts under these respective isolated peaks, $N_{\mathrm{iso\_p}}$ and $N_{\mathrm{iso\_pID}}$, are then obtained and a reference ratio $R_{\mathrm{ref}} = N_{\mathrm{iso\_p}}/N_{\mathrm{iso\_pID}}$ is defined. The number of genuine $\alpha + p$ events in the $Q_{\alpha+\mathrm{p}}$ peak that overlaps with the $Q_{\alpha+\mathrm{d}}$ peak is $N_{\alpha+\mathrm{p}} = R_{\mathrm{ref}} N_{p_{\mathrm{ID}}}$ where $N_{p_{\mathrm{ID}}}$ is the number of identified $\alpha + p$ events the peak in the $Q_{\alpha+p_{\mathrm{ID}}}$ spectra that coincides with the $Q_{\alpha+\mathrm{p}}$ peak in question. The $N_{\alpha+\mathrm{p}}$ events attributed to $\alpha + p$ breakup by this method forms a peak in $Q_{\alpha+\mathrm{p}}$, indicated by a blue arrow in Fig. 10(b). It should be noted that the counts $N_{\mathrm{iso\_p}}$ and $N_{\mathrm{iso\_pID}}$ were chosen from peaks as close as possible to the peak in which $N_{\alpha+\mathrm{p}}$ is to be determined. This is because the ratio R_{ref} varies with the efficiency for $\alpha + p$ and $\alpha + p_{\mathrm{ID}}$ detection, which in turn varies with the Q-value of the process. The final Q spectra showing separated contribution from $\alpha + d$ and $\alpha + p$ breakup is shown in Fig. 10(c). A variation of 20% the reference ratio R_{ref} results in uncertainty in $N_{\alpha+\mathrm{p}}$ that equates to 3% uncertainty in the total $\alpha + p$ yield.

[1] I. Tanihata, H. Hamagaki, O. Hashimoto, S. Nagamiya, Y. Shida, N. Yoshikawa, O. Yamakawa, K. Sugimoto, T. Kobayashi, D. E. Greiner *et al.*, Phys. Lett. B **160**, 380 (1985).
[2] I. Tanihata, H. Hamagaki, O. Hashimoto, Y. Shida, N. Yoshikawa, K. Sugimoto, O. Yamakawa, T. Kobayashi, and N. Takahashi, Phys. Rev. Lett. **55**, 2676 (1985).
[3] N. Rowley, G. R. Satchler, and P. H. Stelson, Phys. Lett. B **254**, 25 (1991).
[4] J. X. Wei, J. R. Leigh, D. J. Hinde, J. O. Newton, R. C. Lemmon, S. Elfstrom, J. X. Chen, and N. Rowley, Phys. Rev. Lett. **67**, 3368 (1991).
[5] M. Dasgupta, D. J. Hinde, R. D. Butt, R. M. Anjos, A. C. Berriman, N. Carlin, P. R. S. Gomes, C. R. Morton, J. O. Newton, A. S. de Toledo *et al.*, Phys. Rev. Lett. **82**, 1395 (1999).
[6] M. Dasgupta, D. J. Hinde, K. Hagino, S. B. Moraes, P. R. S. Gomes, R. M. Anjos, R. D. Butt, A. Berriman, N. Carlin, C. R. Morton *et al.*, Phys. Rev. C **66**, 041602(R) (2002).
[7] M. Dasgupta, P. Gomes, D. J. Hinde, S. B. Moraes, R. M. Anjos, A. Berriman, R. D. Butt, N. Carlin, J. Lubian, C. R. Morton *et al.*, Phys. Rev. C **70**, 024606 (2004).
[8] C. Signorini, Z. H. Liu, Z. C. Li, K. E. G. Löbner, L. Müller, M. Ruan, K. Rudolph, F. Soramel, C. Zotti, A. Andrighetto *et al.*, Eur. Phys. J. A **5**, 7 (1999).
[9] V. Tripathi, A. Navin, K. Mahata, K. Ramachandran, A. Chatterjee, and S. Kailas, Phys. Rev. Lett. **88**, 172701 (2002).
[10] Y. W. Wu, Z. H. Liu, C. J. Lin, H. Q. Zhang, M. Ruan, F. Yang, Z. C. Li, M. Trotta, and K. Hagino, Phys. Rev. C **68**, 044605 (2003).
[11] L. F. Canto, P. R. S. Gomes, R. Donangelo, and M. S. Hussien, Phys. Rep. **424**, 1 (2006).
[12] S. Santra, V. V. Parkar, K. Ramachandran, U. K. Pal, A. Shrivastava, B. J. Roy, B. K. Nayak, and A. Chatterjee, Phys. Lett. B **677**, 139 (2009).
[13] D. H. Luong, D. J. Hinde, M. Dasgupta, M. Evers, R. Rafiei, and R. du Rietz, EPJ Web of Conf. **17**, 03002 (2011).
[14] D. H. Luong, D. J. Hinde, M. Dasgupta, M. Evers, R. Rafiei, and R. du Rietz, EPJ Web of Conf. **35**, 05007 (2012).
[15] P. R. S. Gomes, D. R. Otomar, T. Correa, L. F. Canto, J. Lubian, R. Linares, D. H. Luong, M. Dasgupta, D. J. Hinde, and M. S. Hussein, J. Phys. G: Nucl. Part. Phys. **39**, 115103 (2012).
[16] H. Freiesleben, H. C. Britt, J. Birkelund, and J. R. Huizenga, Phys. Rev. C **10**, 245 (1974).
[17] G. R. Kelly, N. J. Davis, R. P. Ward, B. R. Fulton, G. Tungate, N. Keeley, K. Rusek, E. E. Bartosz, P. D. Cathers, D. D. Caussyn *et al.*, Phys. Rev. C **63**, 024601 (2000).
[18] J. L. Québert, B. Frois, L. Marquez, and G. Sousbie, Phys. Rev. Lett. **32**, 1136 (1974).
[19] D. Scholz, H. Gemmeke, L. Lassen, R. Ost, and K. Bethge, Nuc. Phys. A **288**, 351 (1977).
[20] K. Hagino, A. Vitturi, C. H. Dasso, and S. M. Lenzi, Phys. Rev. C **61**, 037602 (2000).
[21] A. Shrivastava, A. Navin, A. Diaz-Torres, V. Nanal, K. Ramachandran, M. Rejmund, S. Bhattacharyya, A. Chatterjee, S. Kailas, A. Lemasson *et al.*, Phys. Lett. B **718**, 931 (2013).
[22] R. Ost, K. Bethge, H. Gemmeke, L. Lassen, and D. Scholz, Z. Phys. **266**, 369 (1974).
[23] D. J. Hinde, M. Dasgupta, B. R. Fulton, C. R. Morton, R. J. Wooliscroft, A. C. Berriman, and K. Hagino, Phys. Rev. Lett. **89**, 272701 (2002).
[24] C. Signorini, A. Edifizi, M. Mazzocco, M. Lunardon, D. Fabris, A. Vitturi, P. Scopel, F. Soramel, L. Stroe, G. Prete *et al.*, Phys. Rev. C **67**, 044607 (2003).
[25] A. Shrivastava, A. Navin, N. Keeley, K. Mahata, K. Ramachandran, V. Nanal, V. V. Parkar, A. Chatterjee, and S. Kailas, Phys. Lett. B **633**, 463 (2006).
[26] R. Rafiei, R. du Rietz, D. H. Luong, D. J. Hinde, M. Dasgupta, M. Evers, and A. Diaz-Torres, Phys. Rev. C **81**, 024601 (2010).
[27] D. H. Luong, M. Dasgupta, D. J. Hinde, R. du Rietz, R. Rafiei, C. J. Lin, M. Evers, and A. Diaz-Torres, Phys. Lett. B **695**, 105 (2011).
[28] R. Rafiei, D. H. Luong, D. J. Hinde, M. Dasgupta, and R. du Rietz, Int. J. Mod. Phys. E **20**, 835 (2011).
[29] A. Diaz-Torres, D. J. Hinde, J. A. Tostevin, M. Dasgupta, and L. R. Gasques, Phys. Rev. Lett. **98**, 152701 (2007).
[30] A. Diaz-Torres, J. Phys. G: Nucl. Part. Phys. **37**, 075109 (2010).
[31] A. Diaz-Torres, Comput. Phys. Commun. **182**, 1100 (2011).
[32] F. A. Souza, N. Carlin, C. Beck, N. Keeley, A. Diaz-Torres, R. L. Neto, C. Siqueira-Mello, M. M. de Moura, M. G. Munhoz, R. A. N. Oliveira *et al.*, Eur. Phys. J. A **44**, 181 (2010).
[33] E. F. Aguilera, E. Martinez-Quiroz, P. Rosales, J. J. Kolata, P. A. DeYoung, G. F. Peaslee, P. Mears, C. Guess, F. D. Becchetti, J. H. Lupton *et al.*, Phys. Rev. C **80**, 044605 (2009).
[34] L. C. Chamon, B. V. Carlson, L. R. Gasques, D. Pereira, C. De Conti, M. A. G. Alvarez, M. S. Hussein, M. A. Candido Ribeiro, E. S. Rossi, Jr., and C. P. Silva, Phys. Rev. C **66**, 014610 (2002).
[35] D. H. Luong, K. J. Cook, E. Williams, M. Dasgupta, D. J. Hinde, R. du Rietz, R. Rafiei, and M. Evers, PoS(NIC XII) 185 (2012).
[36] D. R. Tilley, J. H. Kelley, J. L. Godwin, D. J. Millener, J. E. Purcell, C. G. Sheu, and H. R. Weller, Nucl. Phys. A **745**, 155 (2004).
[37] O. Häusser, A. B. McDonald, T. K. Alexander, A. J. Ferguson, and R. E. Warner, Phys. Lett. B **38**, 75 (1972).
[38] C. Signorini, M. Mazzocco, G. F. Prete, F. Soramel, L. Stroe, A. Andrighetto, I. J. Thompson, A. Vitturi, A. Brondi, M. Cinausero *et al.*, Eur. Phys. J. A **10**, 249 (2001).
[39] S. Santra, S. Kailas, V. V. Parkar, K. Ramachandran, V. Jha, A. Chatterjee, P. K. Rath, and A. Parihari, Phys. Rev. C **85**, 014612 (2012).
[40] D. R. Tilley, C. M. Cheves, J. L. Godwin, G. M. Hale, H. M. Hofmann, J. H. Kelley, C. G. Sheu, and H. R. Weller, Nucl. Phys. A **708**, 3 (2002).
[41] R. Ost, E. Speth, K. O. Pfeiffer, and K. Bethge, Phys. Rev. C **5**, 1835 (1972).
[42] K. O. Pfeiffer, E. Speth, and K. Bethge, Nucl. Phys. A **206**, 545 (1973).
[43] A. B. McIntosh, S. Hudan, C. J. Metelko, R. T. de Souza, R. J. Charity, L. G. Sobotka, W. G. Lynch, and M. B. Tsang, Phys. Rev. Lett. **99**, 132701 (2007).
[44] L. Fortunato and A. Vitturi, Eur. Phys. J. A **26**, 33 (2005).
[45] M. Ray, A. Mukherjee, M. K. Pradhan, R. Kshetri, M. S. Sarkar, R. Palit, I. Majumdar, P. K. Joshi, H. C. Jain, and B. Dasmahapatra, Phys. Rev. C **78**, 064617 (2008).
[46] P. K. Rath, S. Santra, N. L. Singh, R. Tripathi, V. V. Parkar, B. K. N. K. Mahata, R. Palit, S. Kumar, S. Mukherjee, S. Appannababu *et al.*, Phys. Rev. C **79**, 051601(R) (2009).
[47] M. K. Pradhan, A. Mukherjee, P. Basu, A. Goswami, R. Kshetri, S. Roy, P. R. Chowdhury, M. S. Sarkar, R. Palit, V. V. Parkar *et al.*, Phys. Rev. C **83**, 064606 (2011).